

Article

Study on Soil Corrosion Resistance Reinforced with Reactive Powder Concrete in Chloride Environment

Haozhen Wang ¹, Xin Cai ¹, Xi Peng ^{2,3,*} , Hui Wang ^{1,*} and Pengqian Wang ¹¹ School of Civil Engineering and Geographical Environment, Ningbo University, Ningbo 315000, China² School of Civil Transportation Engineering, Ningbo University of Technology, Ningbo 315211, China³ Engineering Research Center of Industrial Construction in Civil Engineering of Zhejiang, Ningbo University of Technology, Ningbo 315048, China

* Correspondence: pengxi@nbut.edu.cn (X.P.); wanghui4@nbu.edu.cn (H.W.)

Abstract: The accumulation of residue soil (generally composed of soil, residue, or mud consolidation) is one of the important causes of damage to the environment limiting urban development. At present, the recycling rate of residue soil in developed countries is as high as 90%, while in China it is less than 5%. In marine construction, reinforced concrete often suffers from corrosion, which leads to a decrease in the service life and durability of the structure. Reactive powder concrete (RPC) with high strength and good corrosion resistance can solve these problems. In order to efficiently dispose of residue soil, protect the environment, and promote urbanization development, this study uses residue soil as a raw material to replace some cement in RPC, and studies the corrosion resistance of it (under dry–wet alternations and freeze–thaw cycles). In this study, five types of reinforced RPC with different residue soil contents (0%, 2.5%, 5%, 7.5%, and 10%) are prepared. Firstly, the working performance of blank freshly mixed residue soil RPC slurry is analyzed. Then, the corrosion resistance of residue-soil-reinforced RPC under the dry–wet alternations with 3% NaCl and freeze–thaw cycles is analyzed through parameters such as mass loss rate, electrical resistivity, ultrasonic velocity, AC impedance spectroscopy, and Tafel. The results show that under the dry–wet alternations, when the residue soil content is 10%, the corrosion rate and corrosion depth of the residue-soil-reinforced RPC are the minimum, at 43,744.84 g/m²h and 640.22 mm/year, respectively. Under the freeze–thaw cycles, the corrosion rate and corrosion depth of the 10% residue soil content group are higher than that of the 5%, being 52,592.87 g/m²h and 769.71 mm/year, respectively. Compared to the other groups, the reinforced RPC with 10% residue soil content shows good corrosion resistance in both dry–wet alternations and freeze–thaw cycles. Replacing some of the cement in RPC with residual soil to control the amount of residual soil at 10% of the total mass of RPC can effectively improve the corrosion resistance of residue-soil-reinforced RPC and maximize the consumption of residue soil. This plan provides a feasible method for residue soil treatment in the construction industry, while also providing inspiration for research on the corrosion resistance of concrete in marine buildings.



Citation: Wang, H.; Cai, X.; Peng, X.; Wang, H.; Wang, P. Study on Soil Corrosion Resistance Reinforced with Reactive Powder Concrete in Chloride Environment. *Coatings* **2023**, *13*, 1134. <https://doi.org/10.3390/coatings13071134>

Academic Editor: Peter Rodič

Received: 29 May 2023

Revised: 19 June 2023

Accepted: 20 June 2023

Published: 22 June 2023

Keywords: residue soil; RPC; dry–wet alternations; freeze–thaw cycles; corrosion resistance

Copyright: © 2023 by the authors. Licensee MDPI, Basel, Switzerland. This article is an open access article distributed under the terms and conditions of the Creative Commons Attribution (CC BY) license (<https://creativecommons.org/licenses/by/4.0/>).

1. Introduction

Construction residue soil is an important part of construction waste, which is generally composed of soil, residue, or mud consolidation. Research shows that, with the acceleration of the global urbanization process, the construction industry has produced a large amount of residue soil, and billions of tons of residue soil are treated annually [1]. The residue soil will occupy land, pollute the environment, and affect urban development if it is not treated. Furthermore, the recycling rate of residue soil in developed regions, such as the European Union, South Korea, the United States, and Japan, is as high as 90% or above, while in contrast, the comprehensive recycling rate of residue soil in China is no more than 5% [2–4]. The low recycling rate of residue soil in China has become a serious problem. In addition,

marine buildings suffer from serious corrosion by the corrosive environment [5–7], and ordinary reinforced concrete will be corroded and destroyed after 10 to 30 years in the ocean [8–10]. These factors can lead to a decrease in the service life and durability of marine buildings, and even their collapse. Ge [11] mentioned that using silicon powder instead of cement in reactive powder concrete (RPC) can improve its strength, impermeability, and corrosion resistance. Kočí [12] proposed that the compressive strength of RPC can usually reach 200 MPa and it can maintain the integrity of the structure for a long time. In this regard, reactive powder concrete (RPC) [13–15], which has the characteristics of ultra-high strength, high toughness, and durability, may become the key to solving these problems.

At present, there is little research on the corrosion resistance of residue soil concrete around the world. Yu and Wang [16] found that the compressive strength and flexural strength of cement mortar will deteriorate when residue soil is added into the cement. Moreover, it shows the highest and lowest strength when the residue soil content is 5% and 15%, respectively. Wei [17] studied the influence of residue soil content on the performance of C30 concrete. The research showed that the initial slump flow of concrete decreased with the increase in residue soil content.

RPC corrosion resistance is judged by chloride ion permeability. There is little research on the corrosion resistance of RPC doped with residue soil around the world; however, one study [18] measured the diffusion coefficient of chloride ions of RPC with the NEL method as $22.17 \times 10^{14} \text{ m}^2/\text{s}$.

For reinforced concrete, there is a lot of research on corrosion resistance around the world. Green [19] found that there is a linear relationship between the reinforcement corrosion rate and the chloride ion content on the reinforcement surface. Feng [7] studied the corrosion propagation behavior of steel reinforcement using a novel custom-designed wire beam electrode (WBE) covered with uncracked and cracked mortar. The study showed that the WBE technique can effectively monitor passivation and pitting corrosion, especially for the propagation of corrosion. To sum up, there is a lot of research on residue soil concrete, including the working and mechanical properties of RPC around the world. However, there are few studies on the corrosion resistance of residue-soil-reinforced RPC. There are also few relevant reports on its corrosion resistance in the marine environment.

The corrosion of steel bars is an electrochemical process [20]. The passive film on the surface of reinforced concrete in marine construction is constantly eroded by chloride ions. This leads to dullness and the corrosion of reinforced concrete. After the failure of passive films, the exposed iron base forms the anode and a large passive area forms the cathode. The anode and cathode finally produce a potential difference. Thus, the corrosion pattern of the small cathode and large anode is formed. At this moment, rust pits will form on the surface of the steel bars, and they will expand rapidly.

The corrosion of reinforced concrete can be reflected through the parameters of electrochemical detection. Among these parameters, the AC impedance spectrum is a more widely used technology. The AC impedance spectrum allows the impedance to vary with the frequency perturbation of the input AC. At different frequencies, the impedance will approach some kind of electrical resistivity or electrical capacitance. Therefore, the core of electrochemical impedance spectrum (EIS) technology can be obtained, in which the entire electrochemistry of the process can be represented by impedance [21–23]. Furthermore, the measured Tafel curve can also indicate the degree to which the electrode potential needs to be changed in order to achieve a given current. Thus, the corrosion degree of reinforcement can be reflected by the ultrasonic velocity, electrical resistivity, AC impedance, and Tafel curve.

In this experiment, five groups of reinforced RPCs are prepared with different residue soil contents (0%, 2.5%, 5%, 7.5%, and 10%). Firstly, the working performance (the setting time and slump flow) of the newly mixed concrete slurry is analyzed. Then, the steel bar is placed into the residue soil RPC to study the parameters of the ultrasonic velocity, the AC electrical resistivity, and the AC impedance spectrum. Finally, the corrosion resistance of RPC in the dry–wet alternations with 3% NaCl and freeze–thaw cycles is analyzed by

using these parameters. This study provides a good scheme for the residue soil reclamation treatment and corrosion resistance research of marine construction.

2. Experimental Procedure

2.1. Raw Materials and Preparation Maintenance

2.1.1. Raw Materials

Ordinary Portland cement P·O42.5, produced by Xiangshan Conch Cement Co., Ltd., Ningbo, China, is applied in this study. P·O cement has an initial setting time of 45 min and a final setting time of 390 min. Additionally, P·O cement has a specific surface area of 365 m²/kg. The residue soil produced by the construction of a subway line in Ningbo is used in this study. Moreover, the residue soil has a particle size of 11 μm and a specific surface area of 190 m²/kg. The aggregate is quartz sand. The particle sizes are 1~0.71 mm, 0.59~0.35 mm, and 0.15~0.297 mm, and the mass ratio of the sand is 1:1.5:0.8. Polycarboxylic acid superplasticizer (SP) is used in this study as an admixture to improve the fluidity of raw material mixing, and the water-reducing rate can reach 40%. The quartz sand and water-reducing agent were produced by Shanghai Yingshan New Material Technology Co., Ltd., Shanghai, China. Reinforcement of 6.5 mm diameter is used in this study, and the steel mesh is made of stainless steel. Table 1 shows the cumulative raw material passing rate of the cement and residue soil. Table 2 shows the chemical composition of the raw materials.

Table 1. Cumulative pass rate of raw materials (%).

Types	Particle Size (%)							
	0.3	0.6	1	4	8	64	360	
Cement	0	0.33	2.66	15.01	28.77	93.59	100	
Residue soil	31.2	41.2	48.8	82.3	100	100	100	

Table 2. Chemical composition of raw materials (%).

Types	Chemical Composition (%)									
	SiO ₂	Al ₂ O ₃	Fe ₂ O ₃	MgO	CaO	SO ₃	R ₂ O	P ₂ O ₅	Organic Matter	Loss
OPC	20.86	5.47	3.94	1.73	62.23	2.66	0.48	0	0	2.63
SAC	46.07	13.68	4.81	3.27	12.09	0.26	4.1	0.31	5.2	11.5

2.1.2. Specimen Preparation and Curing

The residue soil contents of five groups of residue-soil-reinforced RPC prepared in this study are 0%, 2.5%, 5%, 7.5%, and 10%, respectively, with six specimens in each group. The specimens are prepared according to GB/T 50081-2019. All weighed raw materials are poured into a UJZ-15 mortar mixer to be stirred for 40s. Then, the time is recorded, and the initial setting time of the specimens is calculated. The mixed concrete is poured into oiled plastic molds, obtaining specimens with sizes of 50 mm × 50 mm × 50 mm when the slump flow test is completed. All specimens are cured at a temperature of 20 ± 2 °C and a relative humidity above 95% (GB50204-2015) after demolding. All specimens are taken out and numbered after 2 days. Figure 1 shows a diagram of the specimens. Table 3 shows the coordination of each group.

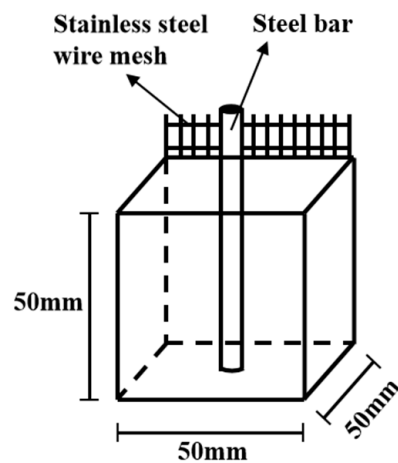


Figure 1. A schematic diagram of the specimen.

Table 3. The mix ratio of concrete.

Group	Water	Cement	Sand	Water Reducer	Residue Soil
1 (0%)	219.9	1466.5	1173.3	47.8	0
2 (2.5%)	219.9	1393.2	1173.3	47.8	73.4
3 (5%)	219.9	1319.9	1173.3	47.8	146.6
4 (7.5%)	219.9	1246.5	1173.3	47.8	219.9
5 (10%)	219.9	1173.3	1173.3	47.8	293.3

Note: The unit is g. The masses of coarse sand, medium sand, and fine sand in each group were 355.5 g, 533.3 g, and 284.4 g, respectively.

2.2. Dry–Wet Alternations and Freeze–Thaw Cycles

The specimens numbered 1, 2 and, 3 in a group are subjected to dry–wet alternations with 3% NaCl and the specimens numbered 4, 5, and 6 are subjected to freeze–thaw cycles with chlorine salt.

To simulate dry–wet alternations with 3% NaCl, specimens are put into the solution (3% NaCl) to soak for 12 h. Subsequently, the specimens are placed into the electric blast drying oven (with the temperature set to 80 °C) for 36 h, with 2 d as a cycle, which is repeated 10 times.

To simulate freeze–thaw cycles of chlorine salts, specimens are put into the freeze–thaw cycle box (temperature range from −18 to 5 °C, with a deviation within 2 °C). One cycle is set for 3 h of freeze–thaw and the cycle repeats 100 times. Furthermore, since the specimen has been wet and saturated during curing before circulation, no additional soaking is required.

2.3. Measurement Method

2.3.1. Measurement of Slump Flow

The slump flow of mixed concrete is measured using the jumping table. The jumping table is produced by Wuxi Prospecting Instrument Factory, Zhejiang Province, and its model number is NLD-3. The power supply voltage of the jumping table is 220 V, the vibration drop distance is 10 mm ± 0.2 mm, the vibration frequency is 1 Hz, and the diameter of the table is 300 mm ± 1 mm. The specific operation process refers to the GB/T 2419-2005 Chinese standard [24].

2.3.2. Measurement of Setting Time

The setting time is determined by the setting time tester in this study. The pressure area of the probe of the setting time tester is 30 mm². Moreover, the initial setting time

corresponds to pressure 0.7 MPa. According to Equation (1), the pressure corresponding to the initial setting time is 21 N.

$$f_p = \frac{N_p}{A_p} \quad (1)$$

In Equation (1), f_p is the pressure corresponding to the initial setting time, A_p is the pressure area of the probe, and N_p is the pressurized pressure.

The specific operation process refers to the GB/T 1346-2011 Chinese standard [25]. Figure 2 shows the setting time tester and concrete specimens.

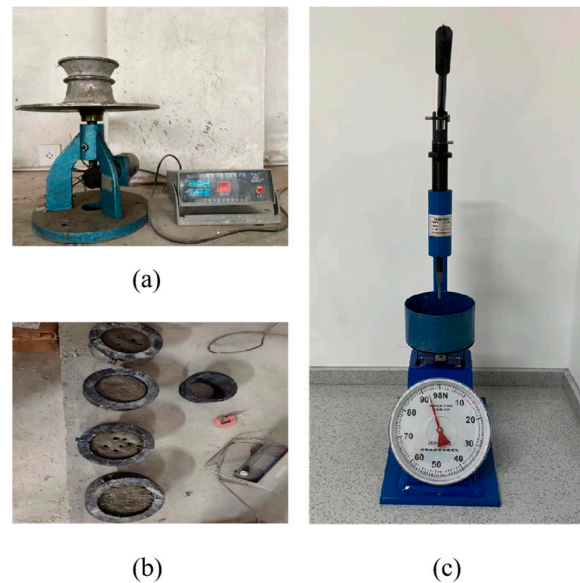


Figure 2. Slump flow and the setting time measurement. (a) Jumping table. (b) Concrete specimens. (c) Setting time tester.

2.3.3. Measurement of Ultrasonic Velocity

Ultrasonic velocity is measured using a JITAI990 ultrasonic detector in this study. The detector can produce sounds ranging from 1000 m/s to 9999 m/s. Vaseline is applied to both sides of the concrete and the probe is stuck on the axis positions. Ultrasonic velocity signals are collected after all of these steps are completed. The detailed measurement process of ultrasonic velocity can be found in Wang's study [26]. Figure 3 is a picture of the JITAI990 ultrasonic detector.



Figure 3. JITAI990 ultrasonic detector.

2.3.4. Measurement of Mass Loss and Electrochemical Parameters

The original rust on the surface of the steel bars is removed by using a sanding process when measuring the mass loss of the specimen. In this study, the original steel bars are then polished with a sand blaster. After polishing, the steel bars are cleaned with citric acid and moved to be dried and weighed. Later, standard cure samples with polished steel bars are applied in the simulated environment. Finally, the mass loss is measured, and the specific measurement process is that of the study of Wang [26].

The AC electrical resistivity is measured using a TH2810D LCR digital bridge. The test voltage is 1 V, and the test frequency is 104 Hz. The steel bar and stainless-steel mesh are used as the two electrodes. Moreover, the digital bridge makes good contact with the electrode. A Princeton electrochemical workstation is used to measure the AC impedance spectrum. The initial AC frequency set in this study is 100,000 Hz, the end AC frequency is 1 Hz, and the voltage is 0.01 V, which meets the conditions of small disturbance. The electrochemical workstation is connected to the electrode of the specimen. The specific measurement process of the AC electrical resistivity and AC impedance spectrum is that of the study of Wang [27]. Figure 4 shows a schematic diagram of the AC electrical resistivity measurement. Figure 5 shows a photo of the electrochemical workstation.

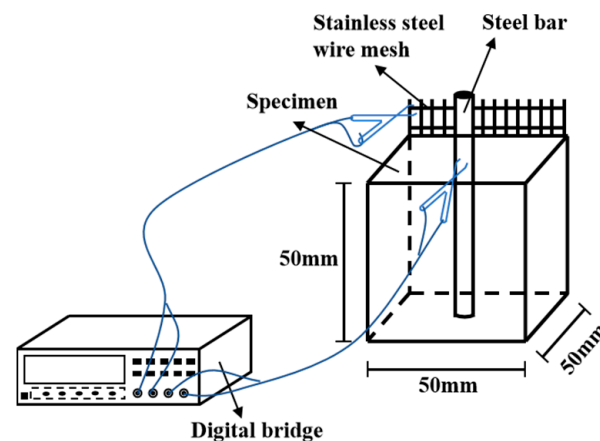


Figure 4. Measurement of the AC electrical resistivity.

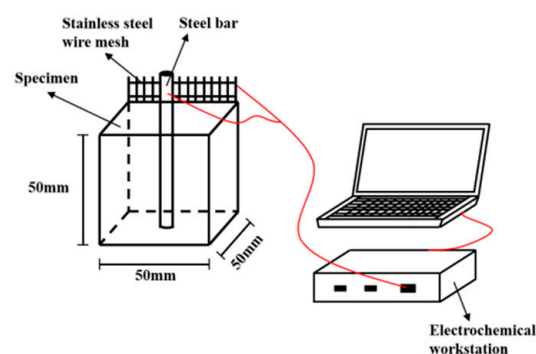


Figure 5. Measurement of the AC impedance spectrum.

3. Results and Discussions

3.1. Working Performance of Residue-Soil-Reinforced RPC

Figure 6 shows the initial setting time (h) and the slump flow (cm) of RPC with different residue soil contents. It can be seen that the initial setting time increases with the increase in residue soil content. The initial setting time changes little when the residue soil content is 0%~5%, and the initial setting time continues to rise when the residue soil content is more than 5%. This is because the residue soil has a much larger surface area than cement in the process of replacing the cement. As a result, the water absorption of

the residue soil is stronger than that of cement [28,29], and it affects the hydration process of cement and prolongs the initial setting time of RPC. The initial setting time increases sharply when the residue soil content changes from 5% to 7.5%. This is because the initial setting time is affected by low ambient temperature when the residue soil content is 7.5%.

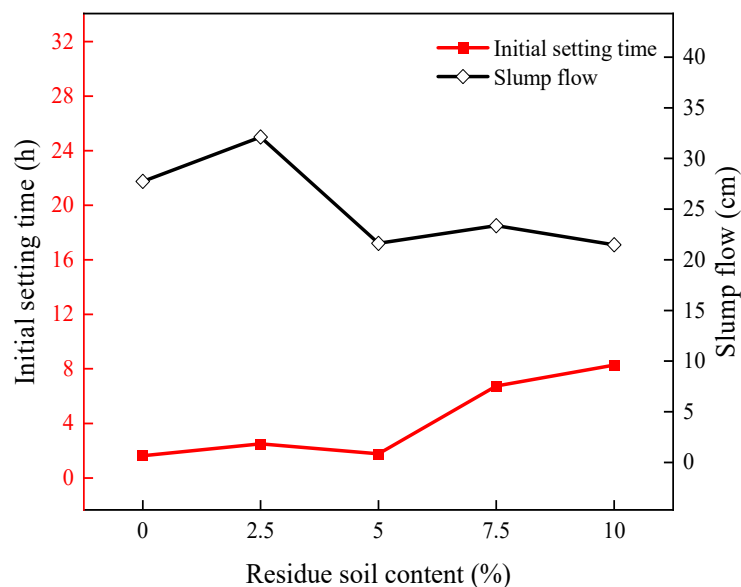


Figure 6. The initial setting time and slump flow with different residue soil contents.

It can also be seen that the slump flow decreased with the increase in residue soil content (from the base of 217.5 mm, slightly increased to 250 mm, and finally dropped to 171 mm). Residue soil has a great influence on the slump flow when its content is less than 5%. Furthermore, when the residue soil content is higher than 5%, the influence is small. This is because the residue soil absorbs the water-reducing agent molecules with the increase in its content [30]. Moreover, water-reducing agent molecules have intercalation in residue soil. The water-reducing agent is consumed by the residue soil, which leads to a reduction in the water-reducing agent acting on the cement and finally results in a reduction in the slump flow.

3.2. Effect of Dry–Wet Alternations on Corrosion Resistance of Residue-Soil-Reinforced RPC

3.2.1. Mass Loss Rate of Residue-Soil-Reinforced RPC

Figure 7 shows the mass loss rate of different residue soil contents during dry–wet alternations. As shown in Figure 7, there is no positive or negative correlation between the residue soil content and the mass loss rate. The mass loss rate of RPC with 5% residue soil content is the lowest. Furthermore, the mass loss rate of RPC with residue soil content in each group and the blank control group increases first and then decreases under the dry–wet alternations. Obviously, there is mass loss after five dry–wet alternations. This is because the steel bars are eroded by chloride ions, which leads to the expansion of the steel bars and the peeling of the concrete surface [31]. The mass loss of 10 dry–wet alternations is not as high as that of 5. This indicates that the mass of concrete after 10 dry–wet alternations is greater than that of 5. This is because the mass loss is greater with the influence of temperature stress when the frequency of dry–wet alternations is low.

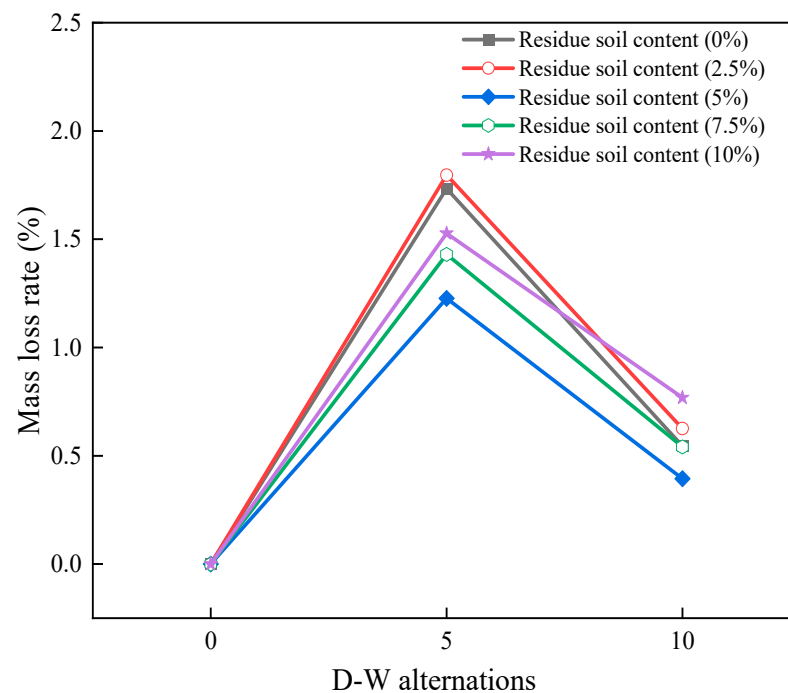


Figure 7. Mass loss rate with different residue soil contents during dry–wet alternations.

3.2.2. Ultrasonic Velocity of Residue-Soil-Reinforced RPC

Figure 8 shows the ultrasonic velocity in different periods. It can be seen from Figure 8 that ultrasonic velocity increases continuously during the curing period. Moreover, ultrasonic velocity reaches the maximum when the curing time is 28 d. In each group, the RPC with 5% residue soil content has the highest ultrasonic velocity, which is 4.45 km/s. The ultrasonic velocity decreases in all of the groups when dry–wet alternation begins. This is because, after repeated immersion in 3% NaCl solution, the chloride ions corrode the steel bars inside of the concrete. This generates rust swelling stress [32] and, because the tensile strength of concrete is less than the rust swelling stress, resulting in cracks appearing inside of the concrete, the ultrasonic velocity decreases [33]. Decky [34] calculates the thermal stress value of cement concrete pavement slabs with a thickness of 12~32 cm and analyzes their sensitivity to different subgrade reaction moduli. The temperature stress level of cement concrete slabs has been determined. When the annual temperature changes from 4.5 to 11.5 °C, a tensile stress in the range of 0.3 to 0.7 MPa will be generated inside of the cement concrete slab. Therefore, temperature stress can also aggravate the cracking of concrete [34,35]. The decrease in ultrasonic velocity before 5 dry–wet alternations is greater than that before 10. This is because the corrosion products of steel bars play a part in filling the micro-cracks in concrete. The reinforced RPC with 5% residue soil content has the largest ultrasonic velocity after 10 dry–wet alternations, which indicates that the reinforced RPC with 5% residue soil content has the largest compaction. The ultrasonic velocity of reinforced RPC with 7.5% residue soil content is the second largest, which is 3.72 km/s. It is close in size to the ultrasonic velocity of reinforced RPC with 10% residue soil content. The ultrasonic velocity of reinforced RPC with 2.5% residue soil content is the smallest, which is 3.52 km/s. This indicates that reinforced RPC with 2.5% residue soil has the smallest compaction. The results are consistent with the mass loss rate chart.

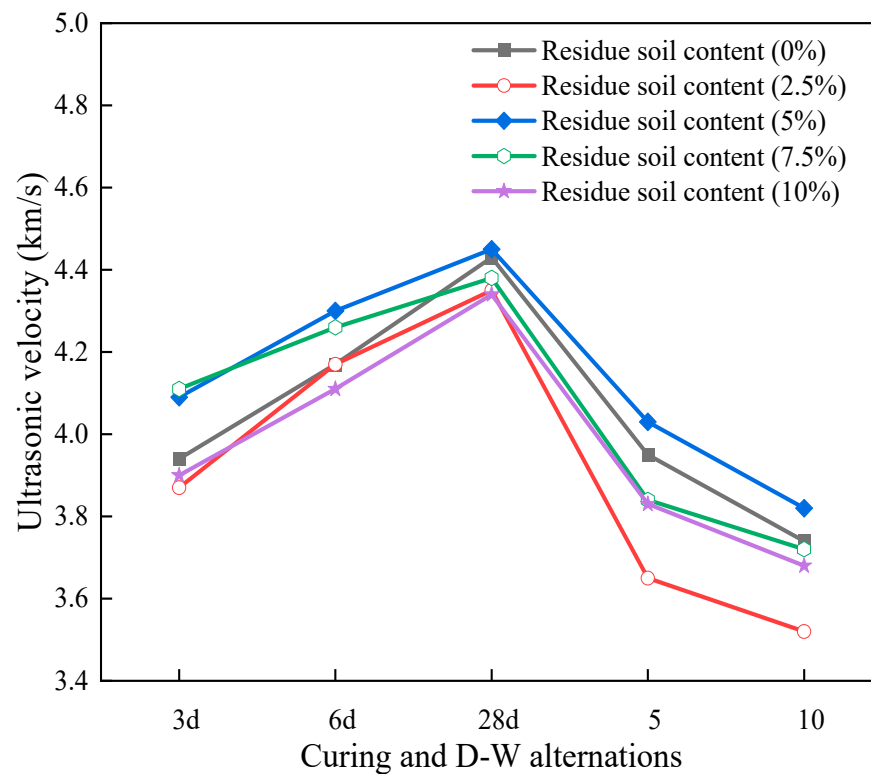


Figure 8. Ultrasonic velocity with different residue soil contents during different periods.

3.2.3. Electrical Resistivity of Residue-Soil-Reinforced RPC

Figure 9 shows the variation of the electrical resistivity in different periods. As shown in Figure 9, the reinforced RPC with 5% and 10% residue soil content have higher electrical resistivity. Furthermore, there is no positive or negative correlation between the residue soil content and the electrical resistivity. The electrical resistivity of each group shows a trend of first decreasing and then increasing again with curing and dry–wet alternations. The electrical resistivity reaches its maximum when the curing time is 28 d. The electrical resistivity of all of the groups decreases after curing for 3 d to 6 d, and the RPC with 5% residue soil content decreases the most. This is because the moisture content in the residue-soil-reinforced RPC increases with the increase in curing time, resulting in the electrical conductivity increasing and the electrical resistivity decreasing. The electrical resistivity of each group increases after curing for 6 d to 28 d. This is because the gradual hydration of the residue-soil-reinforced RPC results in the increase in compactness and the gradual disconnection of pores, which eventually leads to an increase in the electrical resistivity. It can be seen that hydration has a great effect on electrical resistivity. At the beginning of the dry–wet alternations (28 d later), the electrical resistivity begins to decline, which is because the ions in the NaCl solution enter the residue-soil-reinforced RPC and continuously accumulate. At this moment, the electrical resistivity starts to depend on the total amount of charge, and the more the total amount of charge, the lower the electrical resistivity is [36]. The electrical resistivity of all of the groups increases again after five dry–wet alternations. This is because the total charge inside of the residue-soil-reinforced RPC is saturating. Subsequently, hydration is still occurring. At this moment, hydration makes the electrical resistivity increase again.

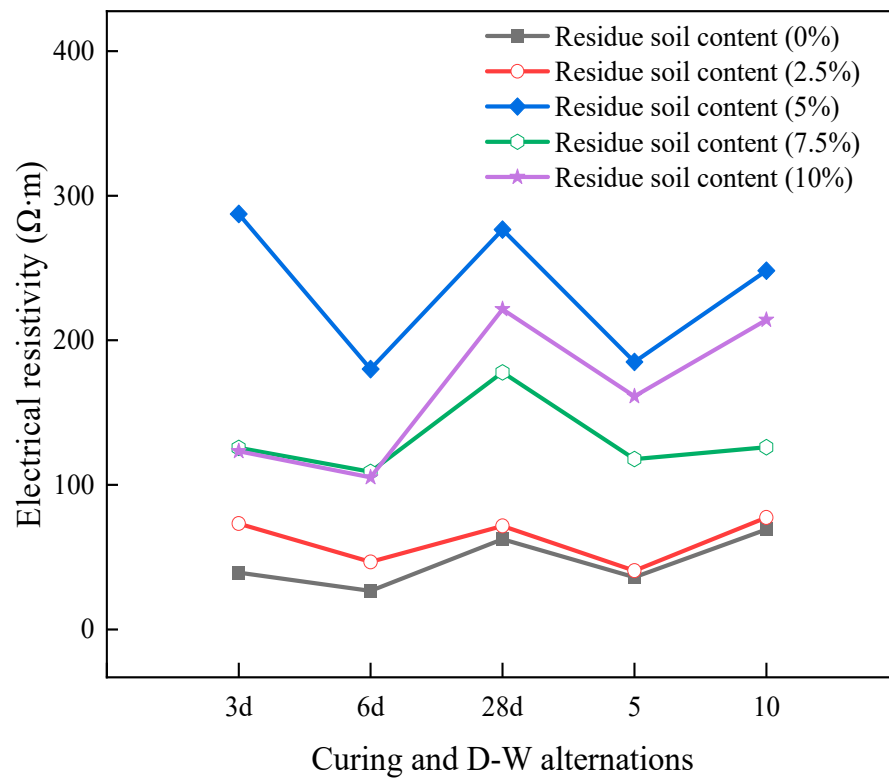


Figure 9. The electrical resistivity of different residue soil contents during different periods.

3.2.4. Electrochemical Performance of Residue-Soil-Reinforced RPC

Figures 10 and 11 show the AC impedance spectrum scatter distribution after 0 and 10 dry–wet alternations, respectively. In Figures 10 and 11, the abscissa Z_r (Ω) represents the electrical resistivity, characterizing the corrosion resistance of the residue-soil-reinforced RPC [37], and Z_i (Ω) represents the electrical reactance.

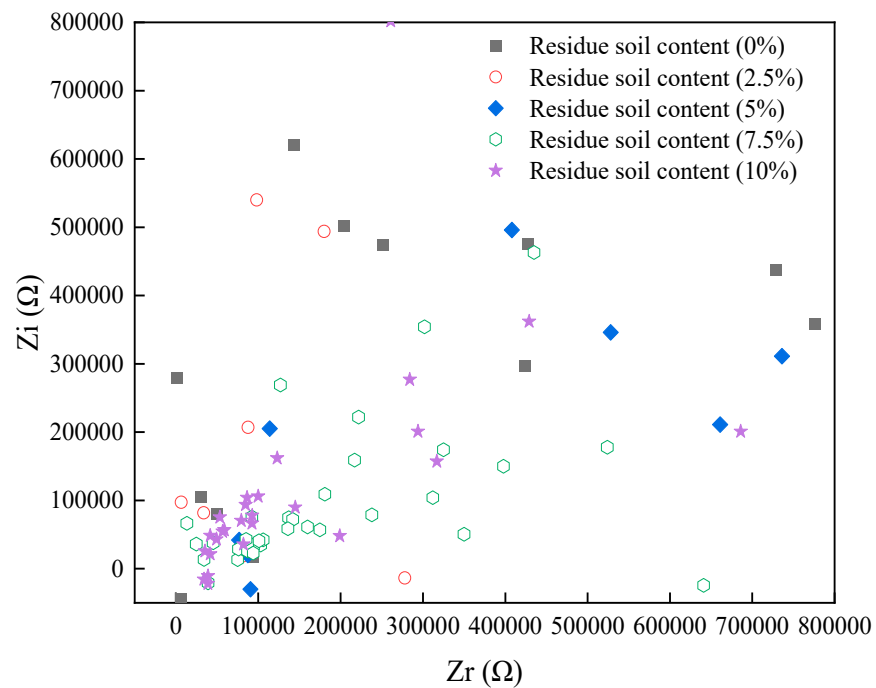


Figure 10. The AC impedance spectrum of 0 dry–wet alternations.

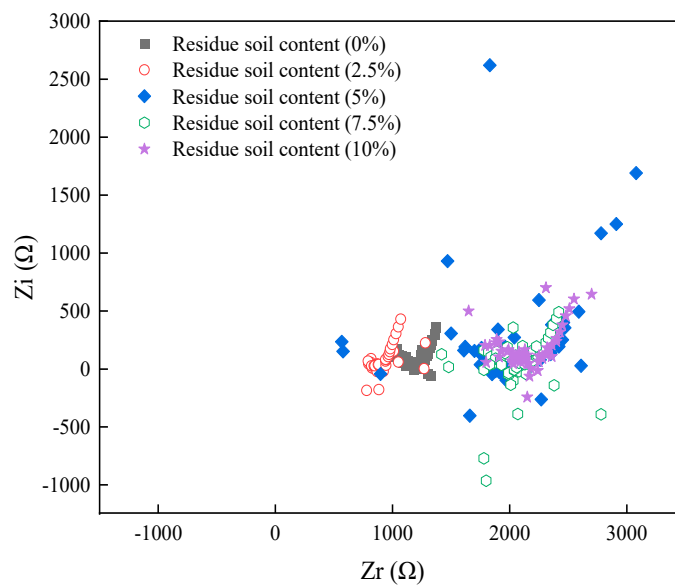


Figure 11. The AC impedance spectrum of 10 dry–wet alternations.

It can be seen from Figure 10 that the impedance values of each group are scattered and irregular after 0 dry–wet alternations. Furthermore, the order of magnitude of the electrical resistivity and the electrical capacitance is extremely large. This indicates that the concrete protective layer of the specimen protects the matrix well and has a strong charge storage ability before the dry–wet alternations [37]. Moreover, the electrical capacitance decreases first and then increases with the increase in the electrical resistivity when the residue soil content is the same. The image moves first to the left and then to the right, and the electrical resistivity value corresponding to the lowest point represents its corrosion resistance with the increase in residue soil content. The higher the electrical resistivity values, the better the corrosion resistance is, which indicates that the residue soil corrosion resistance is better than that of cement. In addition, the corrosion resistance is the best when the residue soil content is 10%. However, the electrical resistivity value of the specimens is smaller than that of the blank control group when the residue soil content is 2.5%. Therefore, concrete with 2.5% residue soil content should be avoided in order to achieve better corrosion resistance in engineering practice.

The corrosion rate of metals can be expressed by the corrosion current density, and the Tafel curve, shown in Figures 12 and 13, can be obtained by converting it with Faraday's law Equations (2) and (3).

$$v = \frac{10M}{n \times \frac{9.65 \times 10^4}{3.6}} \times I = 3.73 \times 10^{-4} \frac{M}{n} I \quad (2)$$

$$d = \frac{v}{\rho} \quad (3)$$

In Equation (2), v stands for the corrosion velocity, and its unit is $\text{g}/\text{m}^2\text{h}$. M represents the atomic weight of the metal, and its unit is g . n represents the atomic valence of the metal. I represents the corrosion current density, and its unit is $\mu\text{A}/\text{cm}^2$. In Equation (3), d indicates the depth of corrosion, and its unit is mm/year . v stands for corrosion velocity, and its unit is $\text{g}/\text{m}^2\text{h}$. ρ represents the density of the metal, and its unit is g/cm^3 .

Figure 12 shows the Tafel curve under 0 dry–wet alternations. Figure 13 shows the Tafel curve under 10 dry–wet alternations. It is not difficult to see that the two branching curves form a complete Tafel curve. The bifurcation point of the curve can reflect the corrosion performance of the specimens [38,39]. It can be seen from Figures 12 and 13 that there is no positive or negative correlation between the residue soil content and the potential of bifurcation points.

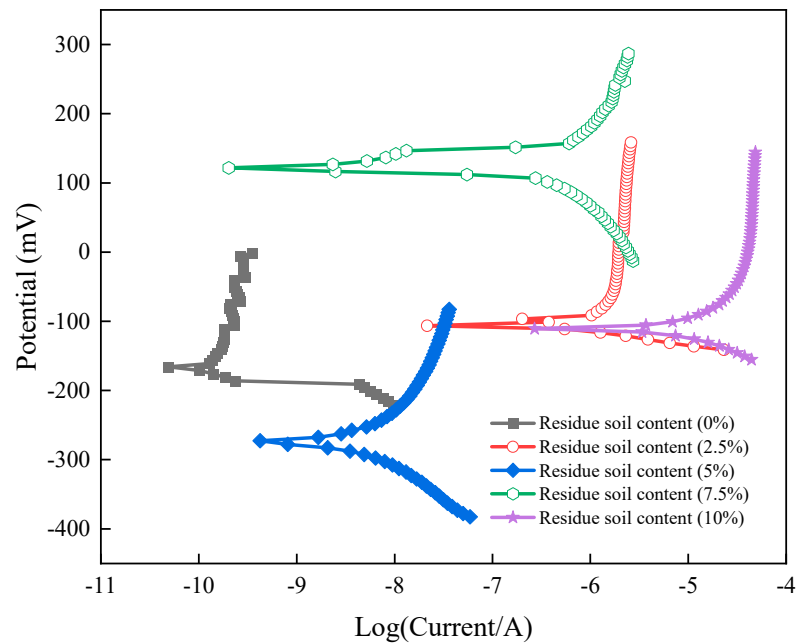


Figure 12. The Tafel curve under 0 dry–wet alternations.

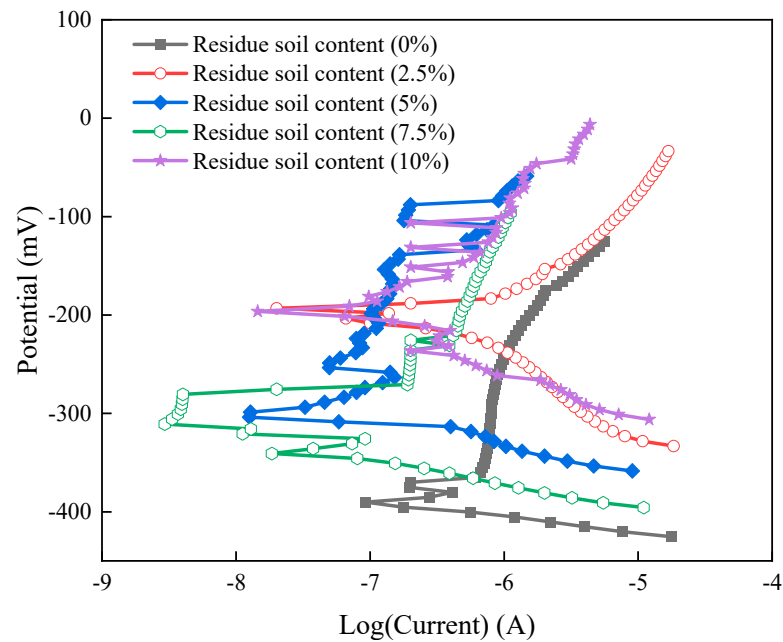


Figure 13. The Tafel curve under 10 dry–wet alternations.

According to the Tafel curve, the voltage and the electrical current of the residue-soil-reinforced RPC in each group are analyzed. Figure 14 shows a bar chart of the corrosion rate and corrosion depth of different residue soil contents under 10 dry–wet alternations. It can be seen from Figure 14 that the corrosion rate and the corrosion depth are not positively correlated with the residue soil content. The corrosion depth of reinforcement increases first and then decreases with the increase in residue soil content. When the residue content is 5%, the maximum corrosion depth is 9043.32 mm/year. When the residue content is 10%, the minimum corrosion depth is 640.21 mm/year. This indicates that residue soil content in a certain range will accelerate the corrosion rate of reinforcement. Moreover, the blank control group and the 10% residue soil content group have better corrosion resistance.

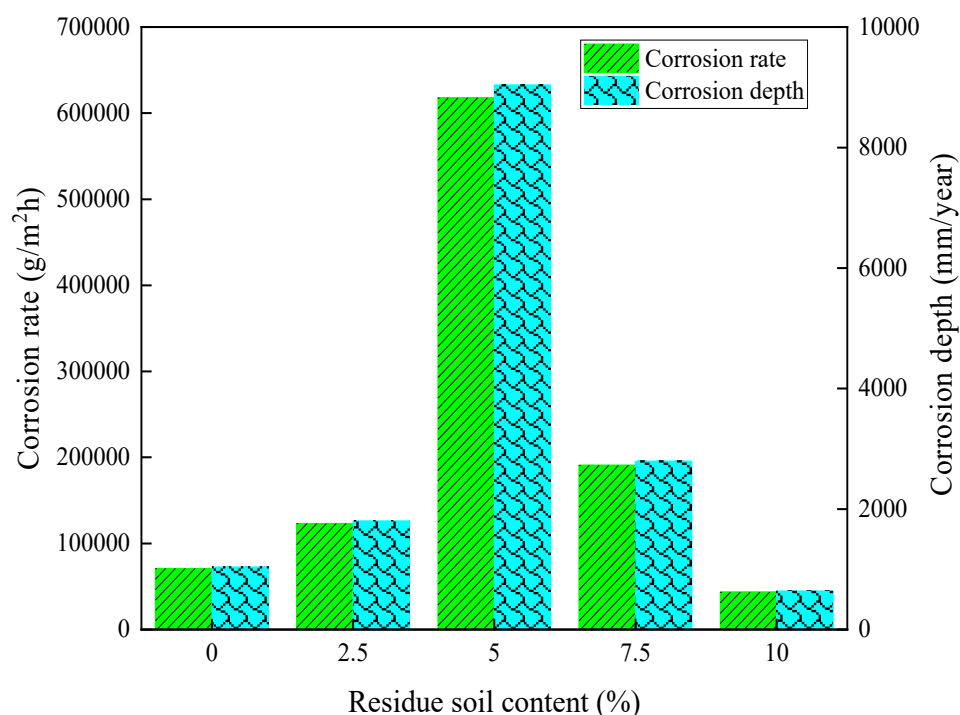


Figure 14. Bar chart of corrosion rate and corrosion depth under 10 dry–wet alternations.

3.3. Effect of Freeze–Thaw Cycles on Corrosion Properties of Residue-Soil-Reinforced RPC

3.3.1. Mass Loss Rate of Residue-Soil-Reinforced RPC

Figure 15 shows the mass loss rate of different residue soil contents during freeze–thaw cycles. It can be seen from Figure 15 that the mass loss rate of each group increases under the freeze–thaw cycle, and when the number of cycles increases from 50 to 100, the mass loss rate increases by an average of 0.72 times. One of the reasons for this is that the NaCl solution inside of the concrete freezes during circulation, resulting in concrete expansion, cracking, and spalling, which finally leads to mass loss [40]. The second reason is that, although the crack is open, the crack also absorbs water instead of part of the mass loss, resulting in the mass loss of 100 cycles being close to, but less than, 1 time. Furthermore, the mass loss rate of reinforced RPC with 10% residue soil content is the smallest. Because the mass loss rate represents the surface erosion of the residue-soil-reinforced RPC and characterizes its corrosion resistance, the reinforced RPC with 10% residue soil content has the best corrosion resistance.

3.3.2. Ultrasonic Velocity of Residue-Soil-Reinforced RPC

Figure 16 shows the ultrasonic velocity during curing and freeze–thaw cycles. It can be seen from Figure 16 that the ultrasonic velocity first increases and then decreases during the curing and freeze–thaw cycles. Moreover, the group with 10% residue soil content and the blank control group have the largest increase. The ultrasonic velocity of each group begins to decrease after the freeze–thaw cycles. The ultrasonic velocity under 100 freeze–thaw cycles is slightly lower than that of 50. This is because the inside of the residue-soil-reinforced RPC is gradually damaged, resulting in micro-cracks, and these micro-cracks grow larger and larger [41]. This is because the ultrasonic propagation velocity in the solution (3% NaCl) with micro-cracks is lower than that in the solid interior of the initial specimen, thus, the ultrasonic velocity decreases [27]. The ultrasonic velocity of the reinforced RPC with 10% residue soil content is the largest, which is 4.24 km/s. Therefore, the RPC with 10% residue soil content has the largest compaction.

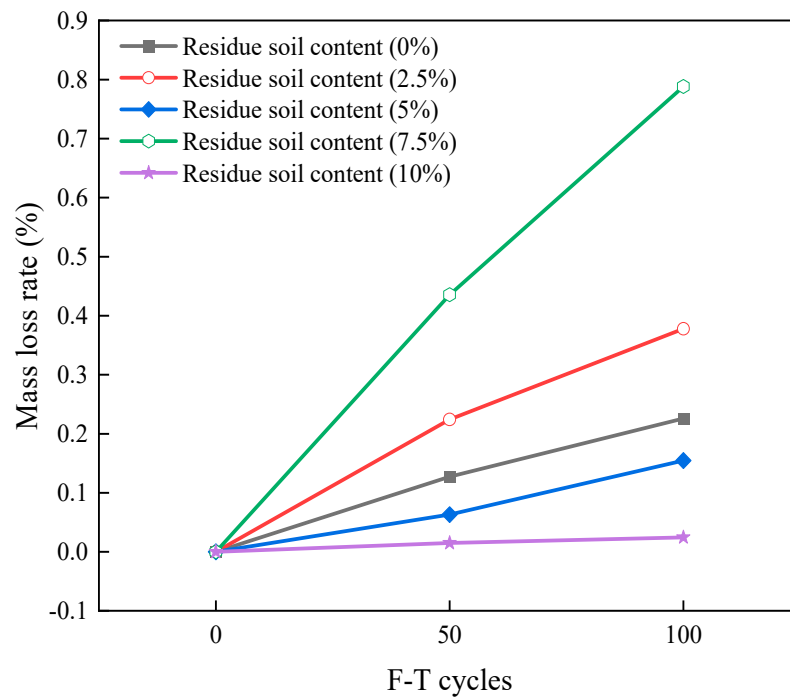


Figure 15. Mass loss rate of different residue soil contents during freeze–thaw cycles.

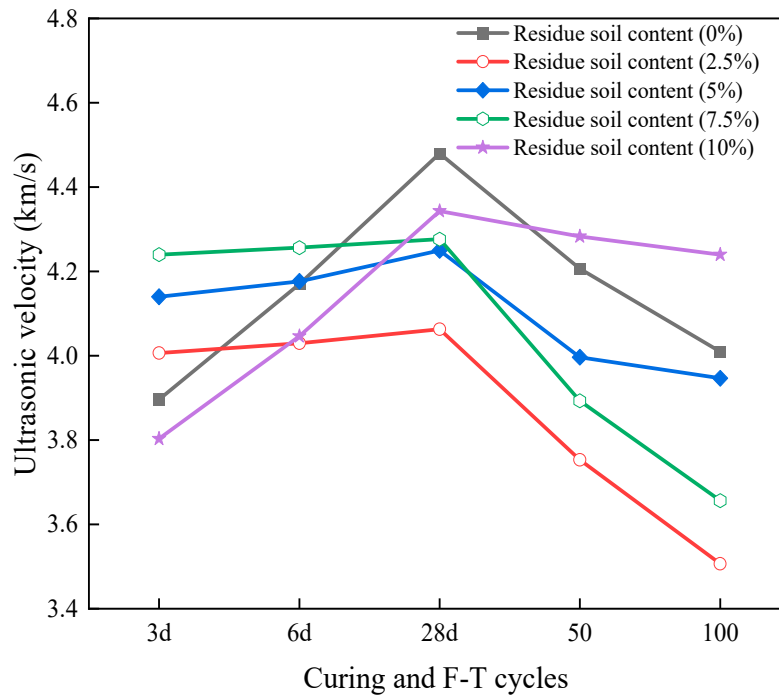


Figure 16. Ultrasonic velocity of different residue soil contents during different periods.

3.3.3. Electrical Resistivity of Residue-Soil-Reinforced RPC

Figure 17 shows the electrical resistivity of each group during different periods. It can be seen from Figure 17 that the electrical resistivity of each group increases with the increase in curing time. Moreover, when comparing 100 freeze–thaw cycles to that of 50, the electrical resistivity growth of each group slows down (5%, 7.5%, and 10%) or even decreases (0% and 2.5%) to different degrees. This is because, although the hydration of concrete is still occurring, the rate of hydration is slower, and the improvement of the concrete compactness is not as significant as it was in the early stage. After 100 freeze–

thaw cycles, the largest electrical resistivity of the group with 7.5% residue soil content is 387.82 $\Omega\cdot\text{m}$, followed by that of 10% residue soil content, which is 319.65 $\Omega\cdot\text{m}$. This indicates that the reinforced RPC with 7.5% and 10% residue soil contents have the better resistance to chloride ion erosion.

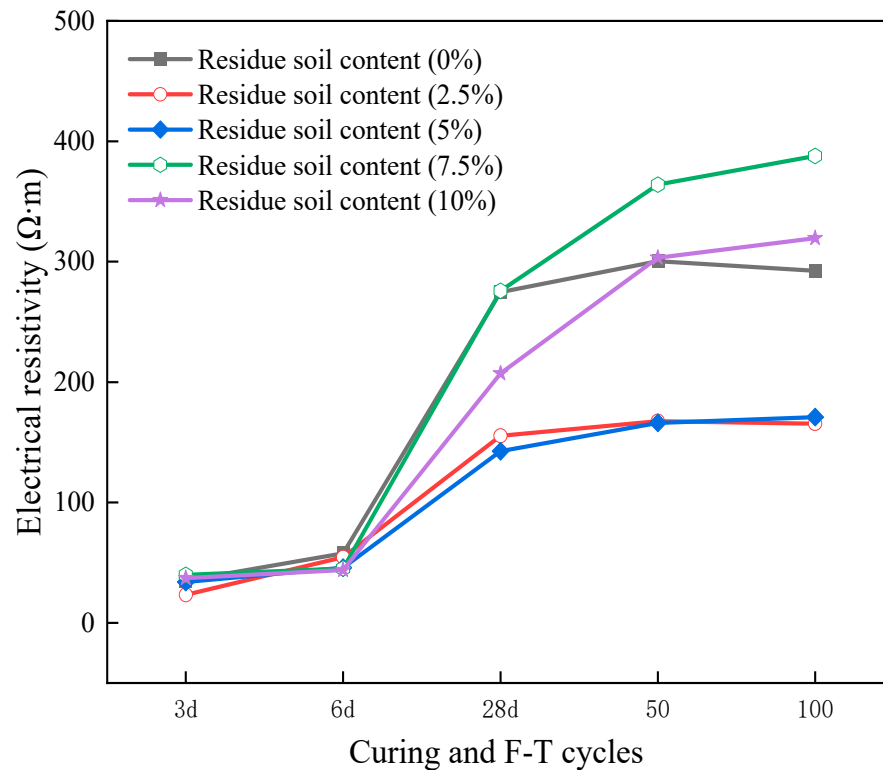


Figure 17. The electrical resistivity of different residue soil contents during different periods.

3.3.4. Electrochemical Performance of Residue-Soil-Reinforced RPC

Figure 18 shows the AC electrical resistivity scatter distribution of 0 freeze–thaw cycles. In the figure, Z_r represents the electrical resistance and reflects the degree of corrosion. As with the dry–wet alternations, the AC impedance scatter distribution of 0 freeze–thaw cycles is irregular. This indicates that the concrete protective layer of the test block before the freeze–thaw cycle protects the matrix well and has a strong charge storage ability.

Figure 19 shows the Tafel curve under 0 freeze–thaw cycles. It can be seen from the curve that mixing residue soil into RPC can effectively improve the corrosion resistance of specimens before the freeze–thaw cycle.

Figure 20 shows a bar chart of the corrosion rate and corrosion depth of different residue soil contents under 0 freeze–thaw cycles. It can be seen from Figure 20 that the annual corrosion depth of the RPCs with 0%, 5%, and 10% residue soil contents is less than 1000 mm, which shows good corrosion resistance.

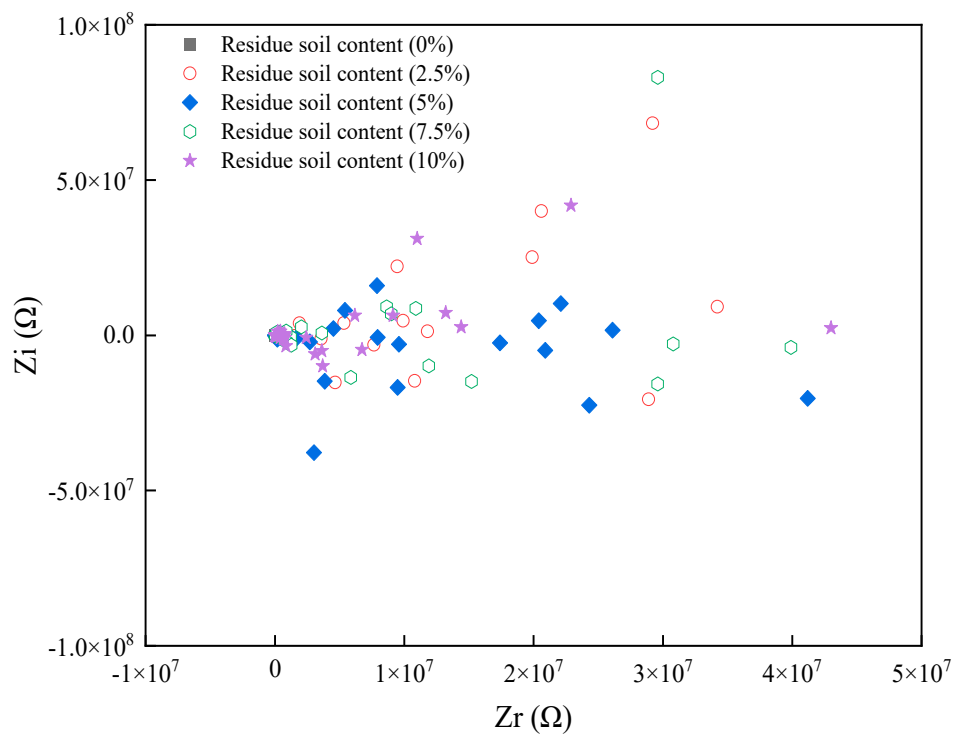


Figure 18. The AC impedance spectrum under 0 freeze–thaw cycles.

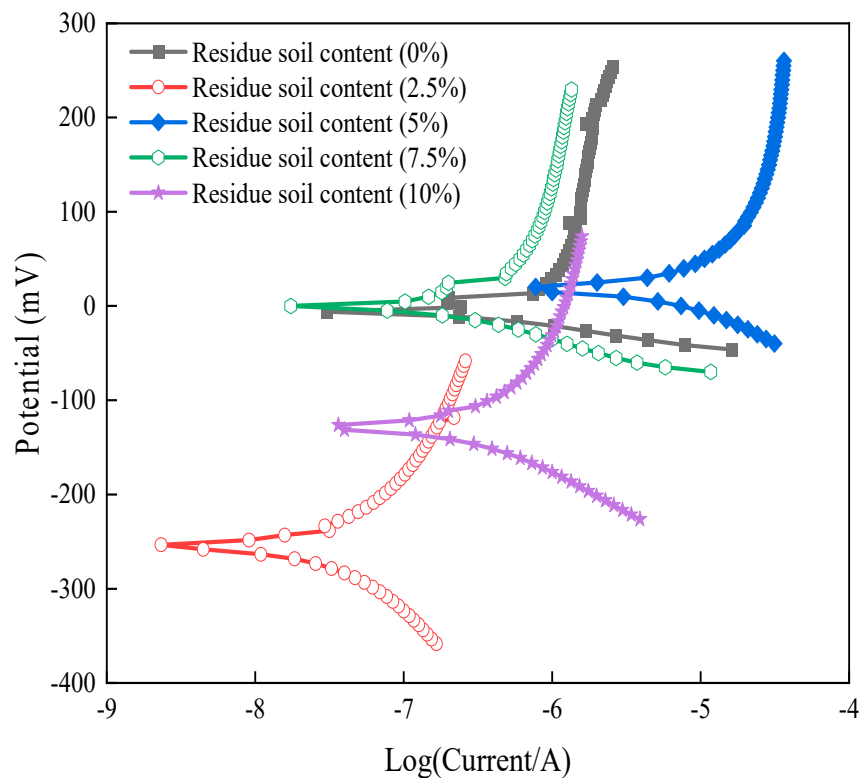


Figure 19. The Tafel curve under 0 freeze–thaw cycles.

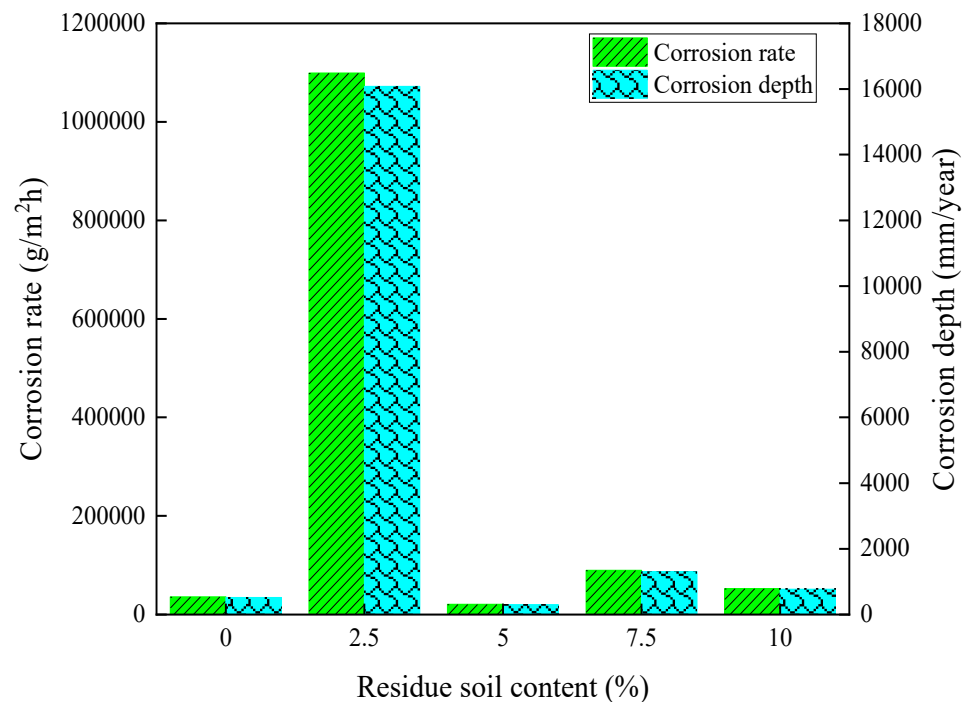


Figure 20. Bar chart of corrosion rate and corrosion depth under 0 freeze–thaw alternations.

4. Conclusions

The multiple properties, including the working performance (slump flow and initial setting time), mass loss rate, and electrochemical parameters (electrical resistivity, ultrasonic velocity, AC impedance spectrum, and Tafel) are analyzed in order to study the corrosion resistance of residue-soil-reinforced RPC. Our research findings can be concluded as follows:

The initial setting time of the residue soil RPC increases with the increase in residue soil content. The slump flow shows a trend of first rising and then falling (from the base of 217.5 mm, then slightly increased to 250 mm, and finally dropped to 171 mm). When the residue soil content is 2.5%, the maximum slump flow is 250 mm, and when the residue soil content is 10%, the minimum slump flow is 171 mm.

The mass loss rate of residue-soil-reinforced RPC increases first and then decreases (when performing dry–wet alternations) and increases (when performing freeze–thaw cycles). The ultrasonic velocity shows the same rule under dry–wet alternations and freeze–thaw cycles. The ultrasonic velocity increases first and then decreases. With the increase in curing age and dry–wet alternations, the electrical resistivity of the residue-soil-reinforced RPC decreases when curing from 3 d to 6 d and then increases when curing from 6 d to 28 d. Moreover, the electrical resistivity decreases (after 28 d) and increases again (after five alternations). Finally, the electrical resistivity reaches its maximum after curing for 28 days. In addition, all of the groups share the same trend. With the increase in curing age and freeze–thaw cycles, the electrical resistivity of the residue-soil-reinforced RPC keeps rising.

The residue-soil-reinforced RPC with 10% residue soil content has good corrosion resistance in both dry–wet alternations and freeze–thaw cycles, which we can see by analyzing the AC impedance spectrum and Tafel curve (a polarization curve that characterizes metals and reflects the relationship between the anodic polarization curve and the current).

Considering the amount of residue soil utilization and corrosion resistance, reinforced RPC with 10% residue soil content is the most suitable for engineering practice due to its high residue soil recycling rate and low corrosion rate. Moreover, reinforced RPC with 2% residue soil content should be avoided in engineering.

Author Contributions: Conceptualization, H.W. (Haozhen Wang), X.P. and H.W. (Hui Wang); Software, P.W.; Validation, H.W. (Haozhen Wang) and P.W.; Formal analysis, H.W. (Haozhen Wang) and X.C.; Investigation, H.W. (Haozhen Wang), X.C. and P.W.; Resources, X.P. and H.W. (Hui Wang); Data curation, H.W. (Haozhen Wang) and X.C.; Writing—original draft, H.W. (Haozhen Wang); Writing—review and editing, H.W. (Haozhen Wang), X.C., X.P. and H.W. (Hui Wang); Visualization, H.W. (Haozhen Wang); Supervision, X.P. and H.W. (Hui Wang); Project administration, X.P. and H.W. (Hui Wang); Funding acquisition, X.P. and H.W. (Hui Wang). All authors have read and agreed to the published version of the manuscript.

Funding: This research was funded by the Natural Science Foundation of Zhejiang Province, China (No. LY22E080005), Ningbo Natural Science Foundation Project (2023J086), and the National Natural Science Foundation of China (52008215).

Institutional Review Board Statement: Not applicable.

Informed Consent Statement: Not applicable.

Data Availability Statement: The data used to support the findings of this study are available upon request.

Conflicts of Interest: The authors declare no conflict of interest.

References

1. Liu, Y.; Lu, H.; Liu, M.; Cai, L.; Wei, N.; Liu, Y. Microanalytical characterizations, mechanical strength and water resistance performance of solidified dredged sludge with industrial solid waste and architecture residue soil. *Case Stud. Constr. Mater.* **2022**, *17*, e01492. [[CrossRef](#)]
2. Xu, S.; He, W. Analysis of Resource Utilization of Construction Residue-Take Ningbo City as an Example. *China Resour. Compr. Util.* **2022**, *08*, 99–101.
3. Ding, Y.; Zhao, J.; Liu, J.; Zhou, J.; Cheng, L.; Zhao, J.; Shao, Z.; Iris, Ç.; Pan, B.; Li, X.; et al. A review of China's municipal solid waste (MSW) and comparison with international regions: Management and technologies in treatment and resource utilization. *J. Clean. Prod.* **2021**, *293*, 126144. [[CrossRef](#)]
4. Song, Q.; Zhu, Z.; Wang, J.; Long, B.; Luo, W.; Jia, Z.; Wang, M. Status Quo of Resource Utilization of Urban Engineering Dregs. *China Resour. Compr. Util.* **2021**, *39*, 90–92.
5. Zhu, P.; Liu, M. Non-uniform Corrosion Mechanism and residual life forecast of marine engineering concrete reinforcement. *J. Eng. Res.* **2023**, *11*, 100053. [[CrossRef](#)]
6. Li, S.; Jin, Z.; Pang, B.; Li, J. Durability performance of an RC beam under real marine all corrosion zones exposure for 7 years. *Case Stud. Constr. Mater.* **2022**, *17*, e01516. [[CrossRef](#)]
7. Feng, G.; Jin, Z.; Zhu, D.; Xiong, C.; Li, Z.; Wang, X. Corrosion propagation of steel reinforcement in pre-cracked mortar attacked by seawater using wire beam electrode. *Corros. Sci.* **2022**, *208*, 110655. [[CrossRef](#)]
8. Shao, W.; Wang, Y.; Shi, D. Corrosion-fatigue life prediction of reinforced concrete square piles in marine environments. *Eng. Fail. Anal.* **2022**, *138*, 106324. [[CrossRef](#)]
9. Xu, J.; Wu, J.; Chen, S.; Diao, B.; Zhao, T. Fatigue life prediction of fatigue damaged and chloride corroded RC beams. *J. Build. Struct.* **2022**, *43*, 69–76.
10. Liu, Q.; Hu, Z.; Lu, X.; Yang, J.; Azim, I.; Sun, W. Prediction of Chloride Distribution for Offshore Concrete Based on Statistical Analysis. *Materials* **2020**, *13*, 174. [[CrossRef](#)]
11. Ge, W.; Wang, A.; Zhang, Z.; Ge, Y.; Chen, Y.; Li, W.; Jiang, H.; Shuai, H.; Sun, C.; Yao, S.; et al. Study on the workability, mechanical property and water absorption of reactive powder concrete. *Case Stud. Constr. Mater.* **2023**, *18*, e01777. [[CrossRef](#)]
12. Kočí, V.; Vejmelková, E.; Koňáková, D.; Pommer, V.; Grzeszczyk, S.; Matuszek-Chmurowska, A.; Mordak, A.; Černý, R. Basic physical, mechanical, thermal and hygric properties of reactive powder concrete with basalt and polypropylene fibers after high-temperature exposure. *Constr. Build. Mater.* **2023**, *374*, 130922. [[CrossRef](#)]
13. Ambika, D.; Nandhini, V.; Santha Rubini, V.; Poovizhi, G.; Dhinu Priya, S. An exploration on the durability properties of reactive powder concrete. *Mater. Today Proc.* **2021**, *45*, 529–534. [[CrossRef](#)]
14. Yang, Q.; Sun, Y.; Peng, X. Experimental Study on Mechanical Properties of Concrete at Super-Early Age. *Materials* **2022**, *15*, 7582. [[CrossRef](#)]
15. Peng, X.; Yang, Q.; Cao, H.; Wang, H. Mathematical Model for Early-Aged UHPFRC Compressive Strength Changes. *Coatings* **2023**, *13*, 525. [[CrossRef](#)]
16. Yu, J.; Zhang, A.; Zhang, L.; Wang, Q.; Li, K.; Wang, H. Study on the performance of low water-binder ratio cement mortar with excavated soil exposed to NaCl freeze-thaw environment. *Mater. Res. Express* **2021**, *8*, 095511. [[CrossRef](#)]
17. Wei, C.; Rong, H.; Song, W.; Qi, Z.; Li, X.; Wang, H. Influence of muck on mechanical properties of C30 concrete. *Concrete* **2016**, *6*, 148–150.

18. Yu, Z.; Gao, K.; An, M.; Han, S. Influence of micro-structure on the strength and resistance to chloride ion permeability of reactive powder concrete. *J. Xi'an Univ. Arch. Technol.* **2013**, *45*, 31–37.
19. Green, W. Steel reinforcement corrosion in concrete—an overview of some fundamentals. *Corros. Eng. Sci. Technol.* **2020**, *55*, 289–302. [[CrossRef](#)]
20. Sun, S. Research on the whole process of corrosion damage of reinforced concrete based on electrochemical impedance spectroscopy. *Shijiazhuang TieDao Univ.* **2020**, 4–7. [[CrossRef](#)]
21. Ejbouh, A.; Ech-chebab, A.; Hassi, S.; Galai, M.; Benqlilou, H.; Touhami, M. Durability assessment of LC³-based reinforced concrete under combined chloride-sulfate environment via the EIS technique. *Constr. Build. Mater.* **2023**, *366*, 130194. [[CrossRef](#)]
22. Ribeiro, D.; Abrantes, J. Application of electrochemical impedance spectroscopy (EIS) to monitor the corrosion of reinforced concrete: A new approach. *Constr. Build. Mater.* **2016**, *11*, 98–194. [[CrossRef](#)]
23. John, D.; Searson, P.; Dawson, J. Use of AC impedance technique in studies on steel in concrete in immersed conditions. *Br. Corros. J.* **2013**, *16*, 102–106. [[CrossRef](#)]
24. GB/T2419-2005; Test Method for Fluidity of Cement Mortar. General Administration of Quality Supervision, Inspection and Quarantine of the People's Republic of China: Beijing, China, 2005.
25. GB/T1346-2011; Test Methods for Water Requirement of Normal Consistency, Setting Time and Soundness of the Portland Cement. General Administration of Quality Supervision, Inspection and Quarantine of the People's Republic of China: Beijing, China, 2011.
26. Wang, H.; Shi, F.; Shen, J.; Zhang, A.; Zhang, L.; Huang, H.; Liu, J.; Jin, K.; Feng, L.; Tang, Z. Research on the self-sensing and mechanical properties of aligned stainless steel fiber reinforced reactive powder concrete. *Cem. Concr. Compos.* **2021**, *119*, 104001. [[CrossRef](#)]
27. Sun, H.; Cheng, W.; Xu, H.; Cai, Z.; Yin, M.; Shi, F. Influence of CO₂ Curing on the Alkali-Activated Compound Mineral Admixtures' Corrosion Resistance to NaCl Dry-Wet Alternations. *Coatings* **2023**, *139*, 67. [[CrossRef](#)]
28. Yang, H. Influence of Mineral Powder and Fiber on Work and Mechanical Properties of Reactive Powder Concrete. *Multipurp. Util. Miner. Resour.* **2023**, *2*, 197–204.
29. Ge, W.; Zhang, Z.; Ashour, A.; Li, W.; Jiang, H.; Hu, Y.; Shuai, H.; Sun, C.; Li, S.; Liu, Y.; et al. Hydration characteristics, hydration products and microstructure of reactive powder concrete. *J. Build. Eng.* **2023**, *69*, 106306. [[CrossRef](#)]
30. Huang, C. Effect of polycarboxylate superplasticizer content on properties of reactive powder concrete. *Adhesion* **2022**, *49*, 116–119.
31. Gong, K.; Wu, M.; Xie, F.; Liu, G.; Sun, D. Effect of dry/wet ratio and pH on the stress corrosion cracking behavior of rusted X100 steel in an alternating dry/wet environment. *Constr. Build. Mater.* **2020**, *260*, 120478. [[CrossRef](#)]
32. Li, R.; Yang, J.; Yang, W.; Liu, Y.; Yang, Z. Degradation Model of Compressive Strength of Concrete under the Action of Steel Bar Rust Expansion. *China Concr.* **2022**, *156*, 16–21.
33. Cui, L.; Wang, H. Research on the Mechanical Strengths and the Following Corrosion Resistance of Inner Steel Bars of RPC with Rice Husk Ash and Waste Fly Ash. *Coatings* **2021**, *11*, 1480. [[CrossRef](#)]
34. Decky, M.; Papanova, Z.; Juhas, M.; Kudelcikova, M. Evaluation of the Effect of Average Annual Temperatures in Slovakia between 1971 and 2020 on Stresses in Rigid Pavements. *Land* **2022**, *11*, 764. [[CrossRef](#)]
35. Liu, Z. Analysis on the Mechanism of Concrete Shrinkage Cracking Under Cooling. *Jiangxi Build. Mater.* **2023**, *1*, 3–8.
36. Wang, H.; Zhang, A.; Zhang, L.; Liu, J.; Han, Y.; Wang, J. Research on the Influence of Carbonation on the Content and State of Chloride Ions and the Following Corrosion Resistance of Steel Bars in Cement Paste. *Coatings* **2020**, *10*, 1071. [[CrossRef](#)]
37. Liang, Z.; Peng, X.; Wang, H. The Influence of Aspect Ratio of Steel Fibers on the Conductive and Mechanical Properties of Compound Cement Reactive Powder Concrete. *Coatings* **2023**, *13*, 331. [[CrossRef](#)]
38. Mei, K.; He, Z.; Yi, B.; Lin, X.; Wang, J.; Wang, H.; Liu, J. Study on electrochemical characteristics of reinforced concrete corrosion under the action of carbonation and chloride. *Case Stud. Constr. Mater.* **2022**, *17*, e01351. [[CrossRef](#)]
39. Zhang, L.; Zhang, A.; Wang, Q.; Han, Y.; Li, K.; Gao, X.; Tang, Z. Corrosion resistance of wollastonite modified magnesium phosphate cement paste exposed to freeze-thaw cycles and acid-base corrosion. *Case Stud. Constr. Mater.* **2020**, *20*, e00421. [[CrossRef](#)]
40. Xia, D.; Yu, S.; Yu, J.; Feng, C.; Li, B.; Zheng, Z.; Wu, H. Damage characteristics of hybrid fiber reinforced concrete under the freeze-thaw cycles and compound-salt attack. *Case Stud. Constr. Mater.* **2023**, *18*, e01814. [[CrossRef](#)]
41. Chen, D.; Deng, Y.; Shen, J.; Sun, G.; Shi, J. Study on damage rules on concrete under corrosion of freeze-thaw and saline solution. *Constr. Build. Mater.* **2021**, *304*, 124617. [[CrossRef](#)]

Disclaimer/Publisher's Note: The statements, opinions and data contained in all publications are solely those of the individual author(s) and contributor(s) and not of MDPI and/or the editor(s). MDPI and/or the editor(s) disclaim responsibility for any injury to people or property resulting from any ideas, methods, instructions or products referred to in the content.